Research Square

Preprints are preliminary reports that have not undergone peer review.
They should not be considered conclusive, used to inform clinical practice,
or referenced by the media as validated information.

Crystal structure of N,N'-bis(tert-butoxycarbonyl)-5,10-dihydrophenazine and periodic DFT- D3(BJ) analysis of the interplay of π-stacking and C-H···O interactions

Lars Walter Weberskirch

boldogi@hhu.de

Heinrich-Heine-Universität Düsseldorf

Research Article

Keywords: dihydrophenazine, crystal structure, lattice energy, periodic DFT, SAPT

Posted Date: November 11th, 2026

DOI: https://doi.org/10.21203/rs.3.rs-11488290/v1

License: This work is licensed under a Creative Commons Attribution 4.0 International License.
Read Full License

Additional Declarations: No competing interests reported.

Crystal structure of N,N'-bis(tert-butoxycarbonyl)-5,10-dihydrophenazine and periodic DFT-D3(BJ) analysis of the interplay of π-stacking and C-H···O interactions

Lars Walter Weberskirch* (https://orcid.org/0009-0005-0884-3744)

Institut für Anorganische Chemie und Strukturchemie, Heinrich-Heine-Universität Düsseldorf, D-40204 Düsseldorf, Germany. E-mail: boldogi@hhu.de

Abstract

The crystal structure of N,N'-bis(tert-butoxycarbonyl)-5,10-dihydrophenazine, a valuable synthetic precursor for phenazine chemistry, and the first example of a carbamate derivative of dihydrophenazine, was determined (triclinic space group $P\bar{1}$ with $Z = 2$). The 5,10-dihydrophenazine core adopts a boat, i.e. *cis*-conformation core, while bulky tert-butyl groups hindering tight packing. Hirshfeld surface analysis shows two groups of interactions, the numerically minor, but relatively stronger CH···O (11.5%) and CH···C (19.7%), which are relatively isolated in comparison to weak H···H (65.7%) vdW interactions. Under these constraints, the concave molecules self-assemble in pairs, with one stronger slip-stacked π···π interaction and two weaker, symmetry-equivalent edge-to-face C-H···π interactions acting cooperatively. Periodic density functional theory (DFT; PBE-D3(BJ), validated against four X23 reference crystals) gives 130.7 kJ mol^{-1} lattice energy, dominated by dispersion. The symmetry-adapted perturbation theory (SAPT) analysis of the symmetry-independent molecular pairs allows direct structural rationalization for the given molecular conformation: four relatively strong pairs were found, the second strongest being the π···π slip stacked pair, whose computed distance closely matches the crystallographic value, although the underlying slip angle differs somewhat. Weaker pairwise interactions, mainly H···H contacts of the tert-butyl groups, contribute little to the lattice energy, isolating the concurrence of the stronger CH···O and CH···C interactions. The SAPT decomposition demonstrates a good structural predictability for weakly interacting dimeric aggregates of dihydrophenazines, while the demonstrated Boc-substituted example represents a general rational approach towards supramolecular dimers for fine-tuning of physico-optical properties.

Keywords: dihydrophenazine, crystal structure, lattice energy, periodic DFT, SAPT

1. Introduction

Phenazine derivatives (Fig. 1) constitute an important class of nitrogen-containing fused aromatic heterocycles with diverse biological, electronic, and physicochemical properties[1–3]. Naturally occurring phenazines exhibit antibacterial, antifungal, antiparasitic, and antitumor activities[1,4], while synthetic derivatives have found applications in medicinal chemistry, catalysis, functional materials, and, more recently, as redox-active components in organic energy-storage devices[5–7].

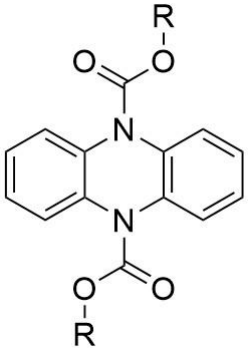


Fig. 1 *General structure of N,N'-disubstituted dihydrophenazine (R_1, R_2 = variable substituents).*

Functionalization at the phenazine nitrogen atoms enables precise modulation of steric and electronic characteristics. Structural characterization of such compounds provides a solid basis for the targeted design of functional materials and offers benchmarks against which quantum-mechanical calculations can be properly validated.

This contribution focuses on N,N'-bis(tert-butoxycarbonyl)-5,10-dihydrophenazine, **1**, a synthetically relevant Boc-protected dihydrophenazine precursor. N-substitution is the central functionalization strategy for phenazines[2]. Compound **1** allows the introduction of multiple amine functionalities via halogenation and Buchwald–Hartwig amination, a strategy relevant to generating electron-rich core phenazines with enhanced luminescent properties.

A search of the Cambridge Structural Database (CSD)[8] revealed ~500 entries containing the 5,10-dihydrophenazine scaffold, yet no carbamates, i.e. $R_2NC(O)OR'$ are reported. The closest analogues, the N-acyl derivatives of 5,10-dihydrophenazines, are also practically unreported, with the sole representative being the 1,1'-(phenazine-5,10-diyl)bis(heptan-1-one),[9] In the latter case, the rationalization of the structure is of secondary interest due to long, flexible alkyl chains, while the more compact, but sterically bulky Boc groups provides a model of limited "supramolecular isolation" disallowing very dense packing.

In this contribution we report the crystal structure of N,N'-bis(tert-butoxycarbonyl)-5,10-dihydrophenazine, **1**, the analysis of its crystal-packing and its rationalization, including QM-calculations.

2. Methods

2.1 Single-Crystal X-ray Diffraction

Single-crystal X-ray diffraction data were collected at 150 K on a Rigaku XtaLAB Synergy Dualflex diffractometer equipped with a HyPix detector using Cu Kα radiation (λ = 1.54184 Å). Data reduction, scaling, and empirical absorption correction were performed with CrysAlis PRO 1.171.43.143a (Rigaku Oxford Diffraction, 2024) using a multi-scan correction based on spherical harmonics implemented in the SCALE3 ABSPACK algorithm.

The structure was solved by intrinsic phasing using SHELXT and refined by full-matrix least-squares refinement on F^2 using SHELXL-2019/3 within the Olex2 environment (version 1.5). Hydrogen atoms were positioned geometrically and refined using a riding model with constrained parameters. Crystal data, data collection parameters, and refinement details are summarized in Table 1. The crystallographic data have been deposited with the Cambridge Crystallographic Data Centre (CCDC 2571096).

Crystal packing was analyzed using DIAMOND (version 5.0.2, Build 47). Hirshfeld surfaces mapped over d-norm and the corresponding two-dimensional fingerprint plots were generated with CrystalExplorer 21.5. Simulated powder X-ray diffraction (PXRD) patterns were generated using Mercury 2026.1.1.

2.2 Computational Methodology

Periodic density functional theory (DFT) calculations were performed with Quantum ESPRESSO 6.6[10,11] using the PBE exchange-correlation functional together with Grimme's DFT-D3(BJ)[12,13] dispersion correction as the primary treatment of dispersion interactions. The non-local rVV10 functional was additionally employed as an independent, non-empirical cross-check[14]. SSSP

1.1.2 (PBE) pseudopotentials were used throughout with plane-wave cutoffs of 60 and 480 Ry for the wavefunctions and charge density, respectively.

Geometry optimizations targeted a force-convergence threshold of 1×10^{-4} Ry Bohr^{-1}, which is stricter than the default Quantum ESPRESSO criterion (1×10^{-3} Ry Bohr^{-1}) commonly applied in molecular-crystal calculations[15] and consistent with the tighter convergence criteria adopted for van der Waals crystal-structure predictions[16]. This criterion was achieved for all structures.

To assess the sensitivity of the dispersion treatment, single-point DFT-D4(BJ)[17] calculations were performed for the X23 reference compounds using the standalone dftd4 program on the D3(BJ)-optimized geometries. The molecular dipole moment of the isolated molecule was additionally calculated with Psi4[18] at the B3LYP/def2-SVP[19] level. MBIS charges were computed with Psi4 (PBE/def2-TZVP). Claude (Anthropic) was used to assist with the software coding of the analysis scripts.

2.3 Electronic Structure and Excited States

Ground-state Kohn-Sham orbitals and vertical singlet excitation energies were calculated with Psi4 at the B3LYP/def2-TZVP level using the PBE-D3(BJ)-optimized isolated-molecule geometry (Section 2.2). The six lowest singlet excited states were computed within the Tamm-Dancoff approximation (TDA-TD-DFT). Canonical frontier orbitals were generated as cube files (three-dimensional grids of the orbital amplitude) and visualized with VMD (version 2.0.0a7)[20] to analyze the spatial character of the dominant electronic transition. State 4 is dominated by few amplitudes, so canonical Kohn-Sham orbitals describe its particle hole character reliably as is established practice[21]. Local and charge-transfer contributions were assessed from the spatial distributions of the frontier orbitals following standard criteria[22].

3. Molecular Structure

The molecular structure of *N,N'-bis(tert-butoxycarbonyl)-5,10-dihydrophenazine* (Fig. 2), synthesized according to the method reported in the Literature[23], shows a distinctly non-planar 5,10-dihydrophenazine core. The crystal structure crystallizes in space group $P\bar{1}$ with $Z = 2$.

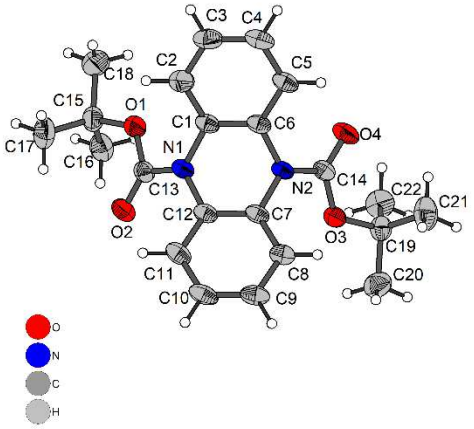


Fig. 2 *Molecular structure of N,N'-bis(tert-butoxycarbonyl)-5,10-dihydrophenazine with ellipsoids drawn at the 50% probability level. Hydrogen atoms are omitted for clarity.*

Table 1 Structure details (CCDC 2571096)

Crystal data	
Chemical formula	$C_{22}H_{26}N_2O_4$
M_r	382.45

Crystal system, space group	Triclinic, $P\bar{1}$
Temperature (K)	150
a, b, c (Å)	10.8735 (2), 10.9484 (2), 11.5251 (1)
α, β, γ (°)	100.388 (1), 104.172 (1), 118.999 (2)
V (Å^3)	1088.77 (4)
Z	2
μ (mm^{-1})	0.65
Crystal size (mm)	0.26 × 0.15 × 0.14
T_{min}, T_{max}	0.481, 1.000
No. of measured, independent and observed [I ≥ 2σ(*I*)] reflections	37829, 4654, 4285
R_{int}	0.041
(sin *θ*/*λ*)$_{max}$ (Å^{-1})	0.637
R[$F^2 > 2\sigma(F^2)$], *wR*(F^2), *S*	0.042, 0.104, 1.05
No. of reflections	4654
No. of parameters	259
H-atom treatment	H-atom parameters constrained
$\Delta\rho_{max}$, $\Delta\rho_{min}$ (e Å^{-3})	0.21, −0.20

The geometrical parameters of both Boc substituents are consistent with carbamate groups. Each Boc group exhibits a short carbonyl bond (C=O: 1.2080(14)-1.2098(15) Å), a longer ester C-O bond (1.4809(16)-1.4812(15) Å), and shortened amide N-C bonds (1.3818(15)-1.3838(16) Å), consistent with the expected amide conjugation. The remaining N-C bonds lie within the normal range for single bonds (1.4300(15)-1.4360(13) Å).

Both Boc substituents adopt a cis arrangement with respect to the dihydrophenazine, placing the carbonyl groups on the same side of the molecule. The aromatic rings are individually nearly planar but folded relative to one another by 136.6°, giving the molecule its characteristic bent geometry. As a result, the crystal packing is dominated by discrete π···π interactions (24.0°), edge-to-face C-H···π contacts (60.0°), and weak C-H···O interactions.

4. Results and Discussion

4.1 Hirshfeld Surface and Intermolecular Interaction Analysis

Mapping the Hirshfeld surface[24] over *d*-norm highlights regions of close intermolecular contact (Fig. 3).

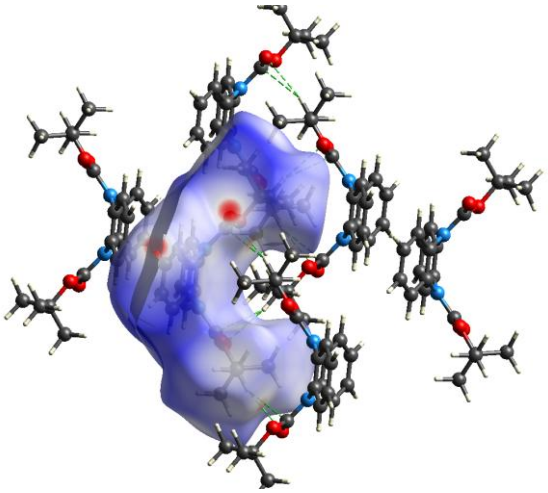


Fig. 3 *Hirshfeld surface mapped over d-norm. Red regions correspond to short C-H···O contacts involving the Boc carbonyl oxygen atoms.*

The Hirshfeld surface shows distinct red d-norm regions at the carbonyl oxygens, identifying the C-H···O contacts as the shortest interactions in the structure, blue regions correspond to longer, weaker van der Waals contacts.

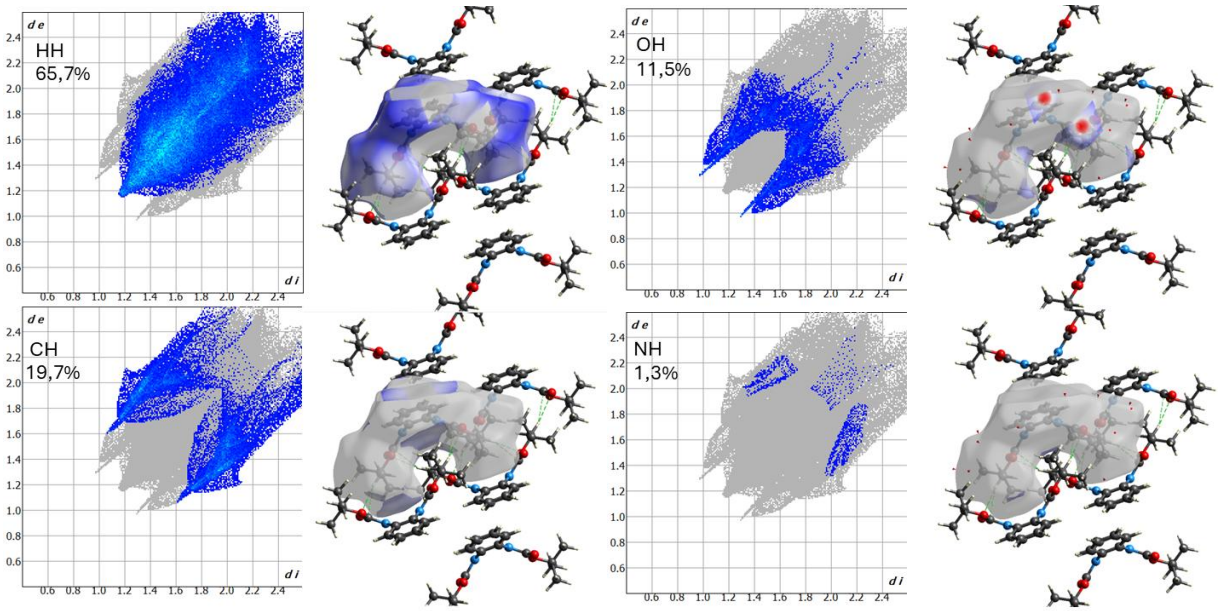


Fig. 4 *Two-dimensional fingerprint plots of the title compound, showing the contributions of H···H (65.7%), C···H (19.7%), O···H (11.5%), and N···H (1.3%) contacts to the Hirshfeld surface.*

Although O···H contacts account for only 11.5 % of the surface (Fig. 4), they produce the characteristic sharp spikes at low d_i and d_e values and represent the closest contacts in the crystal. H···H contacts dominate statistically owing to the high hydrogen content of the molecule; C···H contacts mainly reflect weak C-H···π interactions and efficient packing. The negligible N···H contribution is consistent with complete Boc protection of both nitrogen atoms.

4.2 Crystal Packing

The crystal packing is dominated by C-H···O interactions of the Boc carbonyl groups together with π-stacking contacts, comprising both π···π and C-H···π motifs (Fig. 5).

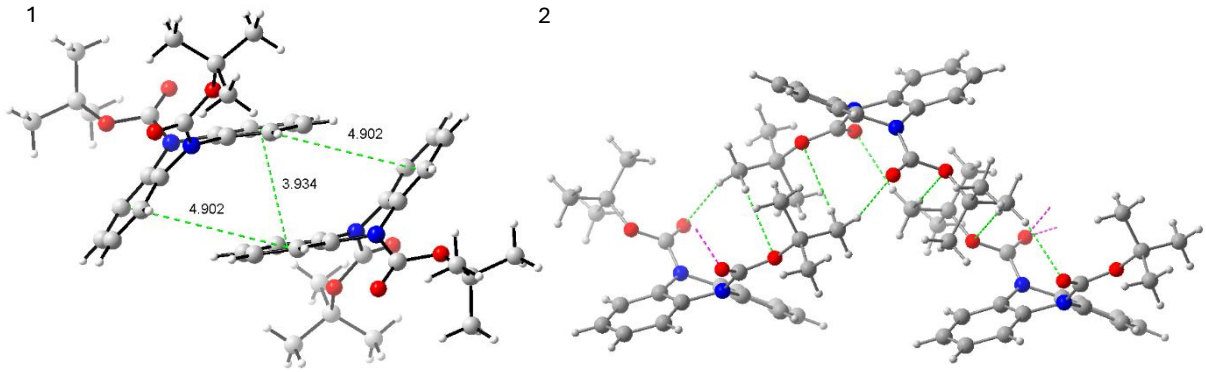


Fig. 5 *Representative intermolecular contacts between neighboring molecules illustrating the π···π stacking and C-H···π motifs for molecules 1 and 2. Green dashed lines highlight the C-H···O hydrogen-bonding contacts that define the intermolecular bridging pattern. Pink lines indicate interactions with additional neighboring molecules not shown in the figure and are included for visual guidance only.*

4.2.1 Geometric Characterization of C-H···π/π···π Contacts

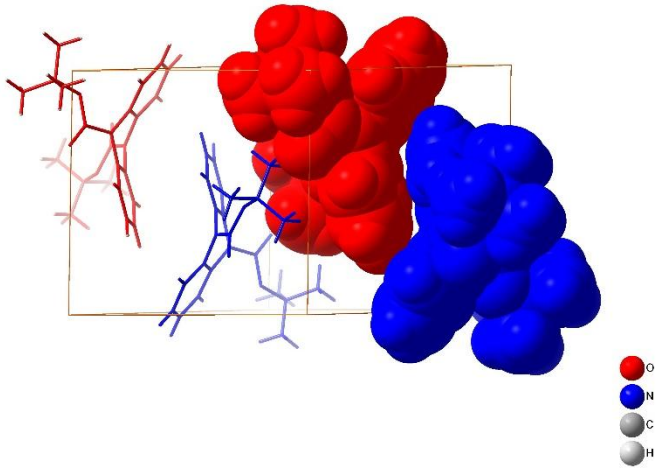


Fig. 6 *Crystal structure highlighting molecule pairs within the unit cell, where all atoms share the same color and only the molecules are differently shaded to emphasize the pairwise arrangement essential for the overall packing.*

The folded geometry of the Boc-substituted dihydrophenazine framework brings neighboring aromatic systems into close proximity, giving rise to two characteristic interaction motifs (Fig. 6). Offset π···π stacking occurs between parallel benzo-rings of adjacent molecules, whereas C-H···π interactions involve an edge-to-face approach of an aromatic C-H group towards the π-system of a neighboring molecule. Rather than forming infinite columns, both motifs generate discrete molecular pairs that constitute the fundamental packing units of the crystal.

For the π···π-stacked pair, the crystallographic centroid distance of 3.934 Å is accurately reproduced by the periodic DFT structure (Section 4.3). The computed slip angle (26.8°) is slightly larger than the experimental value (24.0°), reflecting the geometric coupling of slip and perpendicular separation at fixed centroid distance. The resulting perpendicular distance of 3.513 Å confirms a parallel-displaced rather than an eclipsed stacking arrangement. Re-extracting the pair from the fully relaxed DFT-D3(BJ) structure gives a centroid distance of 3.876 Å and a slip angle of 23.6°, marginally closer to experiment.

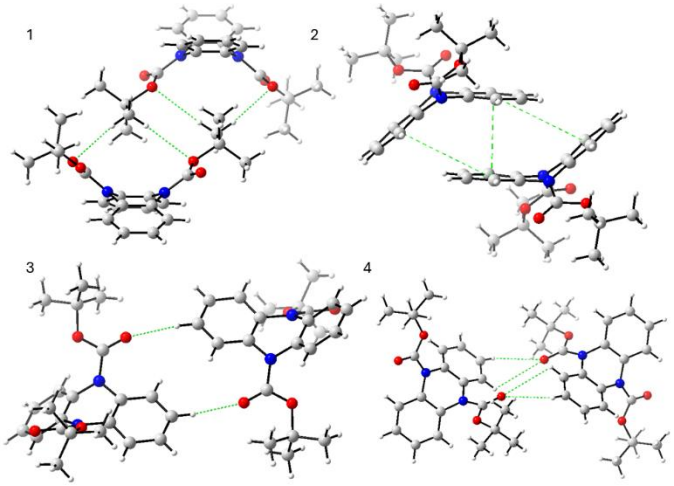


Fig. 7 Overview of the four symmetry-independent molecular pairs (1-4) identified by the nearest-neighbor search and analyzed by SAPT0 (Section 4.3.3) corresponding to (1) the Boc C-H···O + C-H···π-pair, (2) the π···π-stacked pair, (3) the second Boc C-H···O pair, and (4) the tert-butyl···tert-butyl van der Waals pair.

In addition to the aromatic interactions, the Boc carbonyl oxygen atoms participate in several short C-H···O contacts linking neighboring molecular pairs (Fig. 7). Although weaker than classical hydrogen bonds, these contacts reinforce the aromatic interaction network.

4.3 Periodic DFT and Energy Decomposition Analysis

4.3.1 Method validation vs X23 Benchmark

The computational protocol was validated by computing the lattice energy of four molecular crystals from the revised X23 benchmark set[25], selected as structural relatives of the title compound: pyrazine and s-triazine (N-heterocyclic aromatics without N-H), naphthalene (carbocyclic parent), and imidazole (hydrogen-bonded, as contrast) (Table 2).

Table 2 Validation vs X23-Benchmark. All values are given in kJ mol^{-1}.

Compound	PBE-D3(BJ)	PBE-D4(BJ)	X23 Reference	D3 Deviation
Pyrazine	62.45	61.95	64.3[25]	-2.9%
Naphthalene	73.94	78.97	81.3[25]	-9.1%
Imidazole	89.73	97.64	90.4[25]	-0.7%
s-Triazine	57.71	58.49	62.6[25]	-7.8%

The two purely aromatic, non-hydrogen-bonded systems (naphthalene, s-triazine) show the largest deviations (-7.8 to -9.1%), while pyrazine and imidazole agree within 3%. These deviations are within the range reported for PBE-D3(BJ) across the full X23 set[25]. Cutoff convergence can be ruled out as the source of the naphthalene discrepancy, since increasing the cutoff from 80 to 640 Ry changes the result by less than 0.1 kJ mol^{-1}. The remaining deviation is therefore attributed to methodological differences between the present plane-wave/pseudopotential implementation and the PAW-based reference calculations. D3(BJ)/D4(BJ) differ by at most 7.9 kJ mol^{-1}, (imidazole). For pyrazine, rVV10 yields 76.1 kJ mol^{-1}, 21.8% above D3(BJ) and 18.3% above the X23 reference (64.3 kJ mol^{-1}).

4.3.2 Lattice Energy and Term Analysis of Target Compound

For N,N'-bis(tert-butoxycarbonyl)-5,10-dihydrophenazine, the PBE-D3(BJ) electronic lattice energy, $E_{latt} = E_{molecule} - E_{crystal}/Z$, was found to be 130.66 kJ mol^{-1} at the final optimized geometry (Section 2.2). The D3(BJ) correction amounts to 134.6 kJ mol^{-1}, slightly more than the lattice energy itself, i.e. the underlying PBE energy is net repulsive by 3.9 kJ mol^{-1}. Because D3 is an empirical correction rather than the dispersion energy itself, the individual contributions are resolved by the pairwise SAPT0 analysis (Section 4.3.3). A DFT-D4(BJ) single-point check on the D3-optimized geometry yields 132.22 kJ mol^{-1}, 1.56 kJ mol^{-1} (1.2%) higher than the D3(BJ) value.

An independent geometry optimization using the non-local rVV10 functional, yields a substantially higher lattice energy of 180.9 kJ mol^{-1} - 50.2 kJ mol^{-1} (38.5%) above the D3(BJ) value. This agrees with the documented overestimation of molecular crystals by GGA-based rVV10[26], whereas SCAN-rVV10 affords substantially improved accuracy for this class of system[27]. D3(BJ) is therefore adopted as the primary reference lattice energy throughout this work.

The absence of classical hydrogen-bond donors is consistent with a dispersion dominated crystal. For comparison, independent experimental enthalpies of sublimation (ΔH_{sub}) of the parent, unsubstituted phenazine scaffold cluster around 90-100 kJ mol^{-1} [28–30], ΔH_{sub} differs from the 0 K lattice energy by only a few kJ mol^{-1} (typically $\Delta H_{sub} \approx E_{latt} - 2RT$ at 298 K for small, rigid molecules), The two Boc groups add only about 30-40 kJ mol^{-1}, which is modest for two bulky substituents and consistent with inefficient packing of the bulky ter-butyl termini[31].

The isolated molecule has a very small dipole moment (0.19 D), reflecting near-cancellation of the cis-oriented Boc C=O dipoles.

Table 3 SAPT0/jun-cc-pVDZ energy decomposition of the four symmetry-independent, well-localized nearest-neighbor molecule pairs in the crystal (PBE-D3(BJ) geometry). All energies in kJ mol^{-1}; Elst. = electrostatics, Exch. = exchange-repulsion, Ind. = induction. Shortest contact values are given in Å.

Pair	Dominant Motif	Shortest contact	Elst.	Exch.	Ind.	Dispersion	total
1	Boc C-H···O + C-H···π	2.51	-30.0	+49.2	-6.9	-64.6	-52.3
2	π···π stacking (offset)	3.93	-23.7	+48.7	-5.1	-68.5	-48.6
3	Boc C-H···O	2.41	-17.1	+18.1	-5.1	-21.7	-25.8
4	tert-butyl··· (vdW)	2.56-2.62	+0.1	+7.9	-2.3	-18.9	-13.2

Distances refer to the shortest C-H···O atom pair (pairs 1 and 3), the ring centroid distance (pair 2) and the range of shortest H···H contacts (pair 4)

4.3.3 Pairwise Interaction Energies and SAPT Decomposition

An automated symmetry-based nearest-neighbor search (10 Å centroid cutoff) was performed, yielding five symmetry-independent molecular pairs. Four of these are discussed below (Table 3); the fifth, a weak and diffuse ring edge contact, is omitted. For each of the four retained pairsSAPT0/jun-cc-pVDZ provided a decomposition into electrostatic, exchange, induction, and dispersion contributions.

For all four dimers, dispersion is the dominant attractive contribution, confirming the periodic lattice-energy analysis. Electrostatic stabilization is substantial for pairs 1 and 2 (-30.0 and -23.7 kJ mol^{-1}), smaller for pair 3, and essentially absent for the purely aliphatic tert-butyl contact (pair 4). MBIS charges place -0.59 e on the carbonyl oxygens, +0.11 e on each Boc group and -0.22 e on the dihydrophenazine core (gas-phase values differ by ≤0.01 e), so the carbonyl oxygens are the natural acceptors of the C-H···O contacts. SAPT shows that the strongest interaction is not the visually dominant π···π dimer but the Boc-mediated C-H···O + C-H···π.

Because pairs 1 and 2 each combine several simultaneous contact types, isolating the intrinsic strength of π···π stacking versus C-H···π interactions requires reduced model systems. Two models were built by H-capping the relevant ring fragments at their experimental geometry: Model A (both full aromatic ring cores of the π···π-stacked pair, Boc groups replaced by N-H caps) and

Model B (the single Boc-substituted benzo-ring bearing the C-H···π donor, paired with the isolated acceptor ring, both capped at their ring-fusion bonds). At the SAPT2+3/aug-cc-pVDZ level, because the crystallographic inversion center generates two symmetry-equivalent C-H···π contacts flanking the central π···π-stacked ring pair (Fig. 5), the -36.9 kJ mol^{-1} interaction energy of Model A can be approximately partitioned, assuming additivity of the three contact points, into two C-H···π contributions of -9.9 kJ mol^{-1} each (Model B) and a remaining, purely central π···π contribution of approximately -17.1 kJ mol^{-1}. The same partition of the dispersion terms gives -29.0 kJ mol^{-1} (central stack) and -34.8 kJ mol^{-1} (both C-H···π contacts).

This contrasts with the benzene dimer, where parallel-displaced and T-shaped arrangements are nearly isoenergetic[32]. The larger difference observed here is consistent with the well-established increase in π-stacking strength with increasing aromatic surface area, previously demonstrated for larger polycyclic aromatic hydrocarbons[33–35]; the present results extend this trend to the electronically perturbed dihydrophenazine framework studied here.

An extended nearest-neighbor search (15 Å centroid cutoff) identifies several additional, weaker contacts beyond the four principal pairs, including further tert-butyl···tert-butyl and tert-butyl···ring-edge H···H interactions. A few strong pair interactions thus define the primary packing motif, while many weak, less specific van der Waals contacts of the tert-butyl termini fill the remaining space and make up most of the contact surface but only a minor part of the lattice energy.

4.4 Electronic Structure and Excited States

The HOMO is ring-centered, whereas the LUMO is localized on the Boc carbonyls (Online Resource 1); their poor spatial overlap explains the weak HOMO->LUMO transition (State 1, f = 0.021). LUMO+1 and LUMO+3 are ring-centered π*-orbitals (LUMO+1 with a small carbonyl oxygen share) that overlap well with the HOMO. The strongest transition (State 4, ΔE = 4.85 eV, f = 0.164: Table 4) is dominated by HOMO->LUMO+1 (65%) and is best described as a local ring π->π* excitation with a small charge shift away from the carbonyl oxygens, not as charge transfer or mixed π/n.

Table 4 Vertical singlet excitation energies (Δ*E*), oscillator strengths (*f*), and dominant orbital contributions from TDA-TD-DFT (B3LYP/def2-TZVP) calculations on the isolated molecule. Orbital 102 corresponds to the HOMO. Δ*E* values are given in *eV.*

State	Δ*E* (eV)	*f*	Dominant contribution(s)
1	4.458	0.021	HOMO → LUMO (90%)
2	4.755	0.0004	HOMO → LUMO+3 (95%)
3	4.785	0.061	HOMO → LUMO+3 (62%), HOMO → LUMO+1 (24%)
4	4.846	0.164	HOMO → LUMO+1 (65%), HOMO → LUMO+3 (23%)
5	5.360	0.033	HOMO-3 → LUMO (56%), HOMO-1 → LUMO+2 (28%)
6	5.418	0.051	HOMO-1 → LUMO+1 (63%), HOMO-3 → LUMO+3 (13%)

5. Conclusion

N,N'-Bis(tert-butoxycarbonyl)-5,10-dihydrophenazine represents the first crystallographically characterized N,N'-bis(Boc)-protected 5,10-dihydrophenazine. The cis-oriented Boc-substituted molecule has a bent geometry, which prevents the extended π-stacking motifs commonly observed for planar phenazine derivatives while simultaneously introducing carbonyl acceptor sites that participate in weak C-H···O interactions. Periodic DFT gives an estimation for the lattice energy at 130.7 kJ mol^{-1}, dominated by dispersive interactions with the SAPT decomposition of the four symmetry-independent nearest-neighbor pairs confirming the assessment at the pairwise level. While the π···π-stacked dimer represents the most conspicuous structural motif, the strongest pairwise interaction is generated by the cooperative action of a Boc-mediated C-H···O contact and a secondary C-H···π interaction. The boat-shaped conformation is intrinsic to the molecule ,and the carbonyl oxygens carry the largest negative charge (−0.59 e), which rationalizes the C-H···O contacts. The structure and its energetic analysis provide a reference for derivatives accessible from this precursor.

Thereby it is demonstrated that the periodic DFT and SAPT calculations are potentially capable to predict the formation of supramolecular dimers in the Boc-substituted dihydrophenazines, which is foreseen to be a frequent motif for weakly interacting N-substituents, and interesting in the context of engineering materials with fine-tuned physico-optical properties based on property-rich phenazines, particularly in their radical form.

Acknowledgments

This work was carried out within the framework of the CrystSoft course at Heinrich Heine University Düsseldorf (Germany), under the supervision of Dr. István Boldog. The author is grateful to Dr. Boldog for supervising and validating the crystallographic refinement, guiding the structural analysis and presentation, and contributing substantially to the scientific interpretation and revision of the manuscript.

The author thanks Nabil Assahub for synthesizing the compound according to the published procedure and collecting the single-crystal X-ray diffraction data. Computational resources and support were provided by the Center for Information and Media Technology (ZIM) at Heinrich Heine University Düsseldorf, particularly the Hilbert computing cluster, with access facilitated by Prof. Jan Meisner. The author also thanks Daniel Deißenbeck for his critical review of the quantum-chemical methodology.

Funding

No specific funding was received for this research. The work was conducted as part of the regular educational and research activities of the Heinrich Heine University Düsseldorf, using institutional resources.

References

1. Laursen JB, Nielsen J (2004) Phenazine natural products: biosynthesis, synthetic analogues, and biological activity. *Chem Rev* **104**:1663-1686. https://doi.org/10.1021/cr020473j

2. Guttenberger N, Blankenfeldt W, Breinbauer R (2017) Recent developments in the isolation, biological function, biosynthesis, and synthesis of phenazine natural products. *Bioorg Med Chem* **25**:6149-6166. https://doi.org/10.1016/j.bmc.2017.01.002

3. Yan J, Liu W, Cai J, Wang Y, Li D, Hua H, Cao H (2021) Advances in phenazines over the past decade: review of their pharmacological activities, mechanisms of action, biosynthetic pathways and synthetic strategies. *Mar Drugs* **19**:610. https://doi.org/10.3390/md19110610

4. Cimmino A, Evidente M, Mathieu V, Andolfi A, Lefranc F, Kornienko A, Kiss R, Evidente A (2012) Phenazines and cancer. *Nat Prod Rep* **29**:487-501. https://doi.org/10.1039/C2NP00079B

5. Liu Y, Zhang Y, Yang Z, Jing L (2024) Recent advances in phenazine-linked porous catalysts toward photo/electrocatalytic applications and mechanism. *Green Energy Environ* **9**:1518-1549. https://doi.org/10.1016/j.gee.2023.12.006

6. Qi XN, Dang LR, Qu WJ, Zhang YM, Yao H, Lin Q, Wei TB (2020) Phenazine derivatives for optical sensing: a review. *J Mater Chem C* **8**:11308-11339. https://doi.org/10.1039/D0TC01401J

7. Guo M, Li W, Tang W, Tang C, Cao B, He X, Fan C (2025) A p-type small-molecule organic cathode simultaneously for high-voltage Li/Na-based dual-ion full batteries. *Energy Storage Mater* **74**:103979. https://doi.org/10.1016/j.ensm.2024.103979

8. Groom CR, Bruno IJ, Lightfoot MP, Ward SC (2016) The Cambridge Structural Database. *Acta Crystallogr B Struct Sci Cryst Eng Mater* **72**:171-179. https://doi.org/10.1107/S2052520616003954

9. Tang W, Li W (2025) The crystal structure of 1,1'-(phenazine-5,10-diyl)bis(heptan-1-one), C26H34N2O2. *Z Kristallogr New Cryst Struct* **240**:643-644. https://doi.org/10.1515/ncrs-2025-0156

10. Giannozzi P, Baroni S, Bonini N, Calandra M, Car R, Cavazzoni C, Ceresoli D, Chiarotti GL, Cococcioni M, Dabo I, Dal Corso A, de Gironcoli S, Fabris S, Fratesi G, Gebauer R, Gerstmann U, Gougoussis C, Kokalj A, Lazzeri M, Martin-Samos L, Marzari N, Mauri F, Mazzarello R, Paolini S, Pasquarello A, Paulatto L, Sbraccia C, Scandolo S, Sclauzero G, Seitsonen AP, Smogunov A, Umari P, Wentzcovitch RM (2009) QUANTUM ESPRESSO: a modular and open-source software project for quantum simulations of materials. *J Phys Condens Matter* **21**:395502. https://doi.org/10.1088/0953-8984/21/39/395502

11. Giannozzi P, Andreussi O, Brumme T, Bunau O, Buongiorno Nardelli M, Calandra M, Car R, Cavazzoni C, Ceresoli D, Cococcioni M, Colonna N, Carnimeo I, Dal Corso A, de Gironcoli S, Delugas P, DiStasio RA Jr, Ferretti A, Floris A, Fratesi G, Fugallo G, Gebauer R, Gerstmann U, Giustino F, Gorni T, Jia J, Kawamura M, Ko HY, Kokalj A, Küçükbenli E, Lazzeri M, Marsili M, Marzari N, Mauri F, Nguyen NL, Nguyen HV, Otero-de-la-Roza A, Paulatto L, Poncé S, Rocca D, Sabatini R, Santra B, Schlipf M, Seitsonen AP, Smogunov A, Timrov I, Thonhauser T, Umari P, Vast N, Wu X, Baroni S (2017) Advanced capabilities for materials modelling with Quantum ESPRESSO. *J Phys Condens Matter* **29**:465901. https://doi.org/10.1088/1361-648X/aa8f79

12. Grimme S, Antony J, Ehrlich S, Krieg H (2010) A consistent and accurate ab initio parametrization of density functional dispersion correction (DFT-D) for the 94 elements H-Pu. *J Chem Phys* **132**:154104. https://doi.org/10.1063/1.3382344

13. Grimme S, Ehrlich S, Goerigk L (2011) Effect of the damping function in dispersion corrected density functional theory. *J Comput Chem* **32**:1456-1465. https://doi.org/10.1002/jcc.21759

14. Sabatini R, Gorni T, de Gironcoli S (2013) Nonlocal van der Waals density functional made simple and efficient. *Phys Rev B* **87**:041108. https://doi.org/10.1103/PhysRevB.87.041108

15. Cersonsky RK, Pakhnova M, Engel EA, Ceriotti M (2023) A data-driven interpretation of the stability of organic molecular crystals. *Chem Sci* **14**:1272-1285. https://doi.org/10.1039/D2SC06198H

16. Jenkins T, Berland K, Thonhauser T (2025) Van der Waals density functional for molecular crystals. *arXiv* 2509.02358. https://doi.org/10.48550/arXiv.2509.02358

17. Caldeweyher E, Ehlert S, Hansen A, Neugebauer H, Spicher S, Bannwarth C, Grimme S (2019) A generally applicable atomic-charge dependent London dispersion correction. *J Chem Phys* **150**:154122. https://doi.org/10.1063/1.5090222

18. Smith DGA, Burns LA, Simmonett AC, Parrish RM, Schieber MC, Galvelis R, Kraus P, Kruse H, Di Remigio R, Alenaizan A, James AM, Lehtola S, Misiewicz JP, Scheurer M, Shaw RA, Schriber JB, Xie Y, Glick ZL, Sirianni DA, O'Brien JS, Waldrop JM, Kumar A, Hohenstein EG, Pritchard BP, Brooks BR, Schaefer HF III, Sokolov AY, Patkowski K, DePrince AE III, Bozkaya U, King RA, Evangelista FA, Turney JM, Crawford TD, Sherrill CD (2020) PSI4 1.4: open-source software for high-throughput quantum chemistry. *J Chem Phys* **152**:184108. https://doi.org/10.1063/5.0006002

19. Becke AD (1993) Density-functional thermochemistry. III. The role of exact exchange. *J Chem Phys* **98**:5648-5652. https://doi.org/10.1063/1.464913

20. Humphrey W, Dalke A, Schulten K (1996) VMD: visual molecular dynamics. *J Mol Graph* **14**:33-38. https://doi.org/10.1016/0263-7855(96)00018-5

21. Herbert JM (2024) Visualizing and characterizing excited states from time-dependent density functional theory. *Phys Chem Chem Phys* **26**:3755-3794. https://doi.org/10.1039/D3CP04226J

22. Kümmel S (2017) Charge-transfer excitations: a challenge for time-dependent density functional theory that has been met. *Adv Energy Mater* **7**:1700440. https://doi.org/10.1002/aenm.201700440

23. Zeplichal M, Gies J, Bernd J, Kancious Winslaws D, Chang T, Chen YS, Strauss SH, Boltalina OV, Terfort A (2022) Fluorinated azaacenes: efficient syntheses, structures, and electrochemical properties. *J Fluorine Chem* 257-258:109960. https://doi.org/10.1016/j.jfluchem.2022.109960

24. Spackman MA, Jayatilaka D (2009) Hirshfeld surface analysis. *CrystEngComm* **11**:19-32. https://doi.org/10.1039/B818330A

25. Dolgonos GA, Hoja J, Boese AD (2019) Revised values for the X23 benchmark set of molecular crystals. *Phys Chem Chem Phys* **21**:24333-24344. https://doi.org/10.1039/C9CP04488D

26. Tran F, Kalantari L, Traoré B, Rocquefelte X, Blaha P (2019) Nonlocal van der Waals functionals for solids: choosing an appropriate one. *Phys Rev Mater* **3**:063602. https://doi.org/10.1103/PhysRevMaterials.3.063602

27. Dasgupta S, Palos E, Pan Y, Paesani F (2024) Balance between physical interpretability and energetic predictability in widely used dispersion-corrected density functionals. *J Chem Theory Comput* **20**:49-67. https://doi.org/10.1021/acs.jctc.3c00903

28. Sabbah R, El Watik L (1991) Étude thermodynamique de la molécule de phénazine. *Thermochim Acta* **176**:163-171. https://doi.org/10.1016/0040-6031(91)80271-J

29. Leitao ML, Pilcher G, Acree WE Jr, Zvaigzne AI, Tucker SA, Ribeiro da Silva MDCC (1990) Enthalpies of combustion of phenazine N-oxide, phenazine, benzofuroxan, and benzofurazan: the dissociation enthalpies of the (N-O) bonds. *J Chem Thermodyn* **22**:923-928. https://doi.org/10.1016/0021-9614(90)90181-O

30. Arshadi MR (1980) Enthalpies of combustion and formation of phenazine and 2,1,3-benzoxadiazole. *J Chem Thermodyn* **12**:903-906. https://doi.org/10.1016/0021-9614(80)90037-3

31. Chickos JS, Acree WE (2002) Enthalpies of sublimation of organic compounds. *J Phys Chem Ref Data* **31**:537-698. https://doi.org/10.1063/1.1475333

32. Sinnokrot MO, Sherrill CD (2004) Highly accurate coupled cluster potential energy curves for the benzene dimer: sandwich, T-shaped, and parallel-displaced configurations. *J Phys Chem A* **108**:10200-10207. https://doi.org/10.1021/jp0469517

33. Janowski T, Pulay P (2011) A benchmark quantum chemical study of the stacking interaction between larger polycondensed aromatic hydrocarbons. *Theor Chem Acc* **130**:419-427. https://doi.org/10.1007/s00214-011-1009-6

34. Silva NJ, Machado FBC, Lischka H, Aquino AJA (2016) π-π stacking between polyaromatic hydrocarbon sheets beyond dispersion interactions. *Phys Chem Chem Phys* **18**:22300-22310. https://doi.org/10.1039/C6CP03749F

35. Saragi RT, Calabrese C, Juanes M, Pinacho R, Rubio JE, Pérez C, Lesarri A (2023) π-Stacking isomerism in polycyclic aromatic hydrocarbons: the 2-naphthalenethiol dimer. *J Phys Chem Lett* **14**:207-213. https://doi.org/10.1021/acs.jpclett.2c03299

Supplementary Files

This is a list of supplementary files associated with this preprint. Click to download.

- Supplementaryinformation.docx